Cardiovascular Engineering and Technology (© 2017)
DOI: 10.1007/s13239-017-0292-3

Analytical Modeling for Computing Lead Stress in a Novel Epicardial Micropacemaker

LI ZHOU,[1] YANIV BAR-COHEN,[2] RAYMOND A. PECK,[1] GIORGIO V. CHIRIKIAN,[1] BRETT HARWIN,[1] RAMEN H. CHMAIT,[3] JAY D. PRUETZ,[2,3] MICHAEL J. SILKA,[2] and GERALD E. LOEB[1]

[1]Medical Device Development Facility, Department of Biomedical Engineering, Viterbi School of Engineering, University of Southern California, 1042 Downey Way, Los Angeles, CA 90089, USA; [2]Division of Cardiology, Department of Pediatrics, Keck School of Medicine, Children's Hospital Los Angeles, University of Southern California, 4650 Sunset Blvd, Los Angeles, CA 90027, USA; and [3]Division of Maternal-Fetal Medicine, Department of Obstetrics and Gynecology, Keck School of Medicine, University of Southern California, 1300 North Vermont Avenue, Suite 710, Los Angeles, CA 90027, USA

(*Received 5 May 2016; accepted 2 January 2017*)

Associate Editors Timothy Kelley and Ajit P. Yoganathan oversaw the review of this article.

Abstract—Implantation and maintenance of a permanent cardiac pacing system in children remains challenging due to small patient size, congenital heart defects and somatic growth. We are developing a novel epicardial micropacemaker for children that can be implanted on the epicardium within the pericardial space *via* a minimally-invasive technique. The key design configurations include a novel open-coiled lead in which living tissue replaces the usual polymeric support for the coiled conductor. To better understand and be able to predict the behavior of the implanted lead, we performed a radiographic image-based modeling study on a chronic animal test. We report a pilot study in which two mechanical dummy pacemakers with epicardial leads were implanted into an adult pig model *via* a minimally invasive approach. Fluoroscopy was obtained on the animal on Post-Operative Days #9, #35 and #56 (necropsy). We then constructed an analytic model to estimate the *in vivo* stress conditions on the open-coil lead based on the analysis of orthogonal biplane radiographic images. We obtained geometric deformation data of the implanted lead including elongation magnitudes and bending radii from sequenced films of cardiac motion cycles. The lead stress distribution was investigated on each film frame and the point of maximum stress (Mean Stress = 531.4 MPa; Alternating Stress = ± 216.4 MPa) was consistently where one of the leads exited the pericardial space, a deployment that we expected to be unfavorable. These results suggest the modeling approach can provide a basis for further design optimization. More animal tests and modeling will be needed to validate whether the novel lead design could meet the requirements to withstand ~200 million cardiac motion cycles over 5 years.

Address correspondence to Li Zhou, Medical Device Development Facility, Department of Biomedical Engineering, Viterbi School of Engineering, University of Southern California, 1042 Downey Way, Los Angeles, CA 90089, USA. Electronic mail: zhou15@usc.edu

Keywords—Pacemaker, Lead failure, Mechanical analysis, Imaging analysis, Design optimization.

INTRODUCTION

Transvenous pacing is the standard approach to cardiac pacing, and the development of smaller generators and thinner leads have enabled transvenous pacing in children. However, epicardial systems are still needed in selected cases due to difficult venous access, abnormal cardiac anatomy or very small patient size.[14] The implantation and maintenance of these epicardial systems in children remains challenging and major surgery is required for placement (sternotomy or thoracotomy). In addition to these invasive implantation procedures, epicardial lead systems have had inferior long-term outcomes compared to transvenous systems.[5] Furthermore, the cosmetic impact (scarring, skeletal deformities) on those who would not have otherwise needed a thoracotomy can be profound.

In previous studies, we have developed a micropacemaker for use in the human fetus.[9] This is an integrated, single-chamber pacemaker that can be implanted percutaneously into the fetal chest without the need for open uterine surgery. With that experience, it has become clear that the device and implantation technique can be adapted to postnatal use. By implanting a similar device in the pericardial space *via* subxyphoid approach, an entire epicardial pacing system can be implanted percutaneously without the need for thoracotomy or any other surgical incisions.

Published online: 09 January 2017

A non-pacing model of our epicardial micropacemaker system is illustrated in Fig. 1. In this design, the corkscrew electrode is implanted on the epicardial surface of the heart with placement of a miniature pulse generator in the adjacent pericardial or extrapericardial space. Immediately after implantation, the micropacemaker is free to orient itself in a manner that minimizes the mechanical forces to which it is exposed. The short distance between the electrode and the pacemaker housing is connected by an open coil spring made of highly elastic stainless steel (spring tempered SS304 Stainless Steel, wire diameter $d = 152.4\ \mu$m) and insulated with a thin layer of highly flexible and biocompatible polymer Parylene C (thickness = 20 μm). Our lead design takes advantage of the infiltrated, living connective tissue matrix, rather than having the conductor embedded in a synthetic polymer that tends to degrade over time.[12] In many cases, the lead must survive for at least 3–5 years when the child is old enough to receive a conventional transvenous pacemaker. Fatigue failure of the lead is a significant risk over the expected 200 million cardiac cycles. Thus, a lead that can adapt to the local mechanical stresses in the anatomical site is required and a measure of that adaptation can help predict its long-term performance *in vivo*. Helical leads made from spring-like metallic conductors will survive indefinitely if no part of the lead experiences a tensile stress above a fatigue threshold value.[1] Our challenge is to demonstrate that the lead motion observed *in vivo* results in stresses at all points of the lead that stay within the endurance limit of the metal conductor. In this article, we provide a modeling approach to infer stress from observable radiographic motion of such an implanted lead *in vivo*.

MATERIALS AND METHODS

Animal Study

The animal study protocol was approved by the Institutional Animal Care and Use Committee at the University of Southern California. Two mechanical dummy pacemakers were implanted into an adult pig (weight: 32.7 kg) under general anesthesia with 1.5 vol% isoflurane. One device was implanted completely within the pericardial space. The other was placed with the electrode anchored into myocardium, but the pacing lead penetrated through the pericardial membrane to connect to the pacemaker in the extra-pericardial space. Fluoroscopy was performed at implantation and PODs #9, #35 and #56 (necropsy). In each imaging session, we recorded several cycles of cardiac motion in anterior–posterior (AP) and lateral views with a mobile C-arm fluoroscopy machine (Model: Philips Veradius Utility) at 15 frames per second. Necropsy was performed on the POD #56 to evaluate the implant position and tissue interactions by gross dissection and conventional histology (Masson's trichrome stain).

3D Reconstruction of the Implanted Lead

Data Extraction from Radiographic Still Images in Live Animal

The lead motion was captured in sequenced frames of radiographic still images in the AP projection. Orthogonal (lateral) views of comparable cycles of motion were obtained by a 90° rotation of the C-arm of the fluoroscopy machine. The biplane radiological still images (both the AP and lateral) were filtered and contrast-enhanced in the image analysis software Image-Pro Plus® (MediaCybernetics). Due to the machine limitation, the individual coils of the open-coiled spring lead could not be resolved from these radiographic still images. However, the outer contour of the open-coiled lead could be visualized after image processing as illustrated in Fig. 2 (left, inset). A global reference Cartesian coordinate system was established and the origin was anchored on all images at the same position (Fig. 2). The scale dimension in each radiographic image was spatially calibrated based on the actual size of the implants. In the same software environment, a group of 11 equally distant pixel dots (1 mm apart; Fig. 2) was selected on the midline of the open-coiled spring lead. The 2D coordinates (z,y) from AP view and (x,y) lateral view were extracted.

AP and Lateral Image Frames Co-registration

The AP and lateral images could not be obtained simultaneously with the single C-arm fluoroscopy machine. Instead, repetitive lead motion over multiple cardiac cycles at the same heart rate was recorded in separate AP and lateral sequences. The linear distance between two ends of the pacemaker lead was projected onto the common Y axis for the two views (Fig. 2, right). Each AP image was matched with the lateral that had the closest Y projection. After image co-registration, the 3D coordinates were obtained for the 11 data points equally distributed along the midline of the spring. A total of 17 frames of images were analyzed to span more than one complete cardiac cycle.

3D Reconstruction of the Implanted Lead

At each motion frame, the 11 coordinate points on the midline of the open-coiled lead were curve-fitted by applying cubic spline curve interpolation and smoothing functions in MATLAB. The parametric

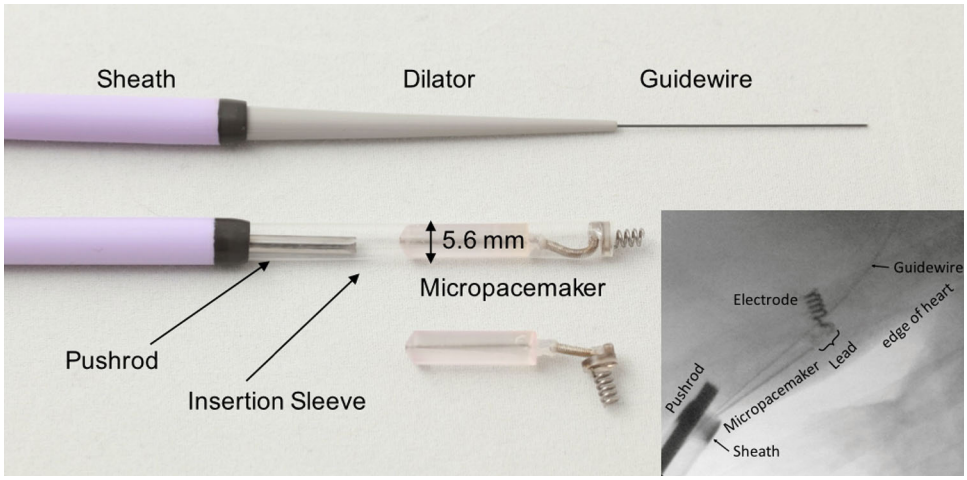

FIGURE 1. The design and mechanical prototype of the epicardial micropacemaker implantation system. To implant the device, a Tuohy needle is introduced under radiographic guidance into the pericardial space *via* subxyphoid approach, a guidewire is advanced into the pericardial space followed by a dilator and sheath (top configuration). The new epicardial micropacemaker device is wedged into the end of an insertion sleeve that allows the corkscrew electrode to be implanted directly into the epicardium (middle configuration). After electrode insertion, the micropacemaker is deployed by a pushrod into the pericardial space (radiographic image inset) and the guidewire, sleeve and sheath are then removed from the body. The micropacemaker system assumes its resting orientation with the myocardial electrode perpendicular to the epicardial lead (bottom configuration).

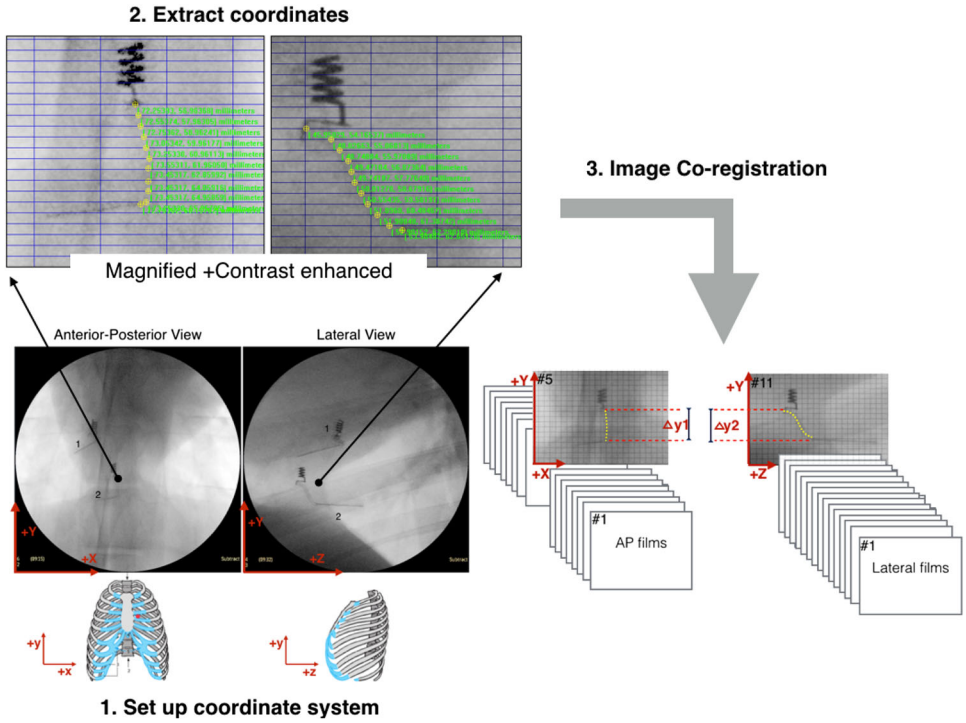

FIGURE 2. The implanted lead coordinates extraction from the radiographic images (projected anterior–posterior and lateral views). Left: Each image was magnified and filtered to increase the contrast. 11 points on the midline of the open-coiled lead were selected. (1) 1st implant in which the corkscrew electrode was implanted directly into the epicardial surface and the entire micropacemaker device was inserted into the pericardial space, but the open-coiled spring lead was kinked during deployment. (2) 2nd implant in which the electrode was again implanted directly into myocardium (in the epicardial space), but the device was deployed after the sheath had exited the pericardial space (and was therefore placed in the pleural space). Right: The anterior–posterior (AP) and lateral radiographic images co-registration process for implant (3). The extracted y coordinates were used to derive the Δy. The criterion to pair the AP and lateral image frames is $\Delta y1 = \Delta y2$. If the criterion is not satisfied, the specific AP recording was advanced to compare with next lateral frames until they match. The process terminates when a sequence of AP and lateral frames was obtained to represent a complete and continuous motion cycle.

representation of the spline was used to interpolate more data points along the midline of the open-coiled lead, which ensures that all the interpolated data points are on the spline curve with a smooth and continuous contour as well as radius of curvature in three-dimensional space (Fig. 3).

The overall deflection of the open-coiled lead could be calculated from the integration of the cubic spline intervals (subtract original known lead length, L_0). Similarly, the 3D radius curvature along the spline could be interpreted with the given parametric function of the curve.[10]

Mathematical Modeling

Our analysis assumes the implanted lead at a motion frame was: (1) stretched to a deflected length; and (2) deformed to the interpreted bending radius of curvatures at each turn of the coil. With the given material properties and existing classic analytic solutions of mechanical springs, the stress resulting from tensile deflection and bending deformation was modeled separately and superimposed together in the material.

For the tensile load alone, analytic prediction of mechanical stresses in the open-coiled lead is based upon Wahl's stress analysis of close-coiled springs.[16] This analytical model can result in reasonable accuracy (error $< 5\%$) in predicting stresses at a spring index $C > 5$ and pitch angle $\alpha < 10°$.[16] The implanted pacemaker lead has a spring structure meeting these requirements, where the spring index $C = 10$ ($C > 5$), and the pitch angle $\alpha = 4.7°$ ($\alpha < 10°$).

The deflection of the open-coiled lead, δ, is the integrated length of the lead midline from the 3D model (section above), where R_0 is the original coil radius. With a known δ, the changes of the pitch angle, α (α_0 = Original Pitch Angle), can be calculated from:

$$\delta = \frac{2\pi R_0}{\cos\alpha_0}(\sin\alpha - \sin\alpha_0)$$

The coil radius after the deflection, R, is given by[16]:

$$\frac{R_0}{R} = \frac{1}{K_2} = \frac{\sin\alpha_0\cos\alpha_0\tan\alpha + (EI/GJ)\cos^2\alpha_0}{\cos^2\alpha\left(\frac{EI}{GJ} + \tan^2\alpha_0\right)}$$

For stainless steel spring of round wire, where the $E/G = 193$ MPa/70 MPa and the $I/J = 2$ (I = moment area of inertia of a spring; J = polar moment area of inertia; E = Young's Modulus (unit in MPa); G = Modulus of Rigidity (unit in MPa)).[16]

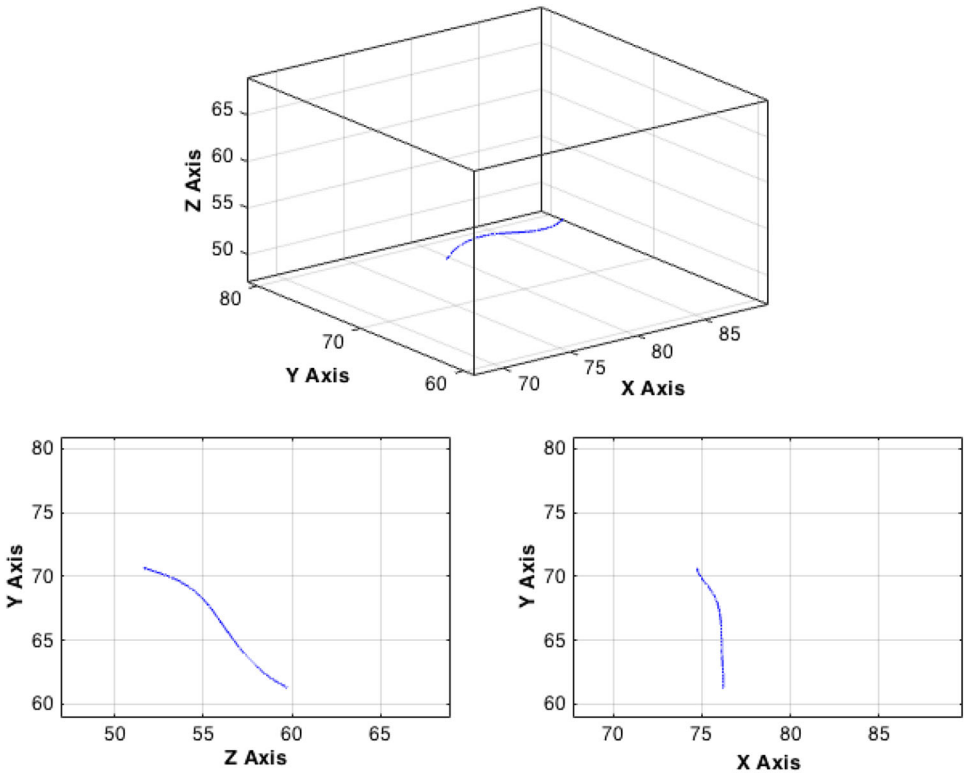

FIGURE 3. The reconstructed implanted lead (midline of the coil) in three-dimensional space. Top: 3D representation of the lead (midline of the coil). The data points along the curve were curve-fitted with cubic spline interpolation with 11 original coordinates extracted from radiographic images. Bottom: the parametric curve fitting in ZY (AP radiographic view) and XY (lateral radiographic view) planes. The interpolated data points fit along the spline in the projected views.

$$R = \frac{1 + 0.767\tan^2\alpha}{1 + 0.767\tan\alpha_0\tan\alpha}\frac{\cos^2\alpha}{\cos^2\alpha_0}R_0$$

The tensile force resulted from the deflection is given by:

$$P = \frac{\delta G d^4}{64K_2(R_0)^3 n}$$

The normal stress, σ, and torsional stress, τ, on the conductor wire circular cross-section are:

$$\sigma = \frac{32PR\sin\alpha}{\pi d^3}$$

$$\tau = \frac{16PR\cos\alpha}{\pi d^3}$$

For the bending load on the close-coiled helical spring, Meaghter *et al.* has developed an analytic model from a strength-of-materials approach proposed by Durelli.[4,7,11] The accuracy of the model was verified with mechanical bending tests of springs and finite element analysis (Fig. 4).[11]

On each particular coil (360° revolution), the torsional and bending components are given by:

$$T_\theta = M\sin\theta\cos\alpha$$

$$M_R = M\cos\theta$$

$$M_z = M\sin\theta\sin\alpha$$

The lateral flexural rigidity, β, is a spring constant. The bending radius of curvature can be anticipated from the parametric function of the 3D cubic spline (see section above). Given a coil of known rigidity, β, and bending radius ρ, the bending moment is calculated from (D = coil diameter, d = wire diameter, r = wire radius)[11]:

$$\frac{1}{\rho} = \frac{M}{\beta} = \frac{2EIGJ\cos\alpha\frac{L}{n}}{D\pi GJ\left[1 + (\sin\alpha)^2\right] + EI(\cos\alpha)^2}$$

Rearrange the equation:

$$M = \frac{\beta}{\rho} = \frac{D\pi GJ\left[1 + (\sin\alpha)^2\right] + EI(\cos\alpha)^2}{2EIGJ\cos\alpha\frac{L}{n}}$$

The torsion T_θ can be calculated. M_{res} is the integration of the M_R and M_z

$$M_{res} = \sqrt{(M\cos\theta)^2 + (M\sin\theta\sin\alpha)^2}$$

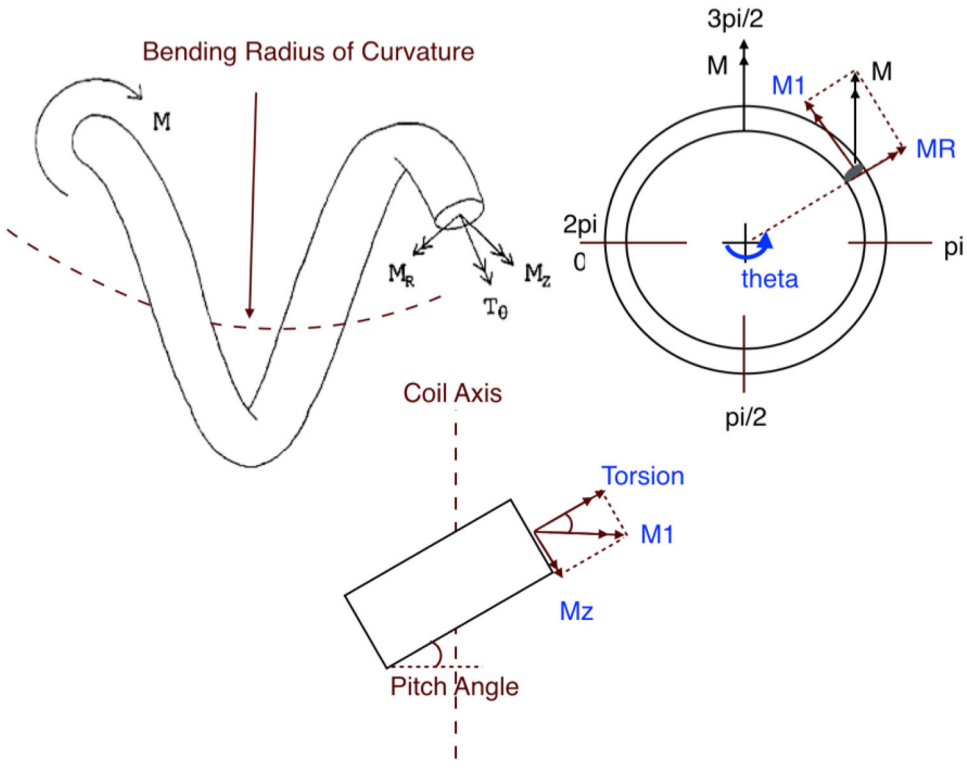

FIGURE 4. Free body diagram of the helical spring subject to bending. M is the overall bending moment on one turn of the coil. M1 and MR (perpendicular to coil axis) are from vector decomposition, which M1 can further resolve into torsion, T_θ and M_z, tangent to the spring wire circular-section (surface perpendicular to the wire axis).

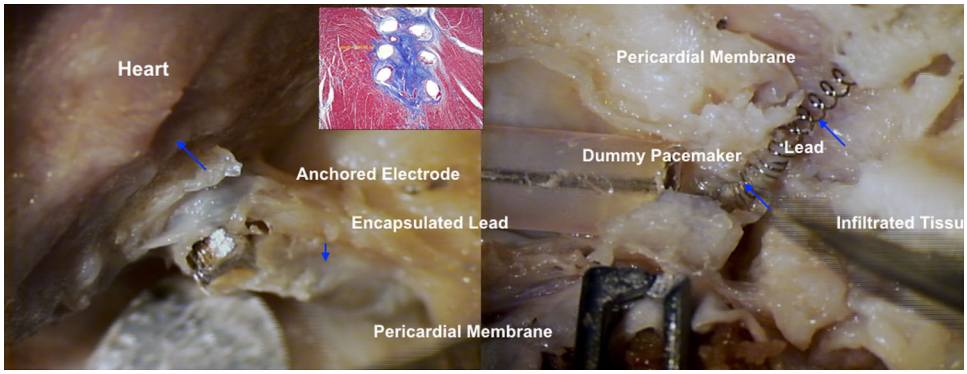

FIGURE 5. The implanted mock pacemaker in an adult pig after 56 days of chronic implantation. Left: the corkscrew electrode (device 2) implanted in ventricular myocardium. Right: the dummy pacemaker in the pleural space. There is moderate epicardial and myocardial fibrosis around both the cylindrical and coil portions of both devices. This fibrous connective tissue reaction exhibited mild chronic inflammation associated with a benign foreign body reaction. The inset photomicrograph illustrates the tissue histology around the iridium electrode in the myocardium.

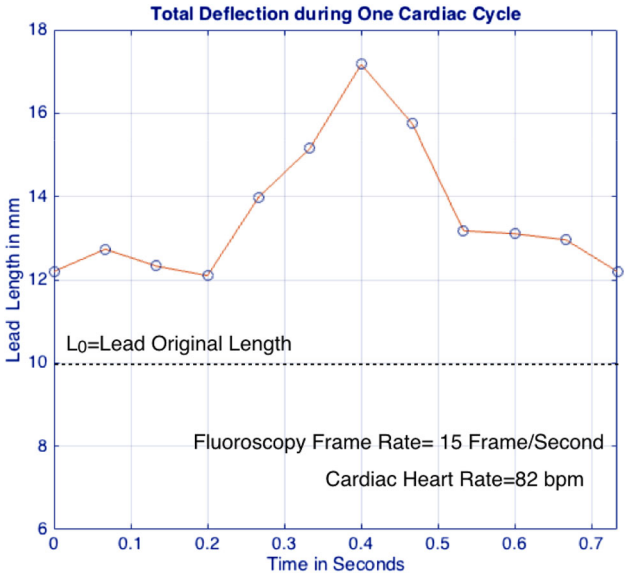

FIGURE 6. Changes in the overall length of the implanted lead during a single cardiac cycle in the pig study. The overall length is obtained from the integration of the 3D cubic spline in each frame. 11 frames represent 1 cardiac cycle.

For the wire with circular cross-section, the curvature stress concentration factor, K, is a function of distance from wire axis, di, where $0 < di < d$. γ is the polar angle on the wire circular cross-section from 0 to 2π[4]

$$K = \frac{4\frac{D}{d}(\sec\alpha)^2 - \frac{d}{2x}}{4\frac{D}{d}(\sec\alpha)^2 - 4\frac{2x}{d}}$$

And

$$x = \frac{d_i}{2}\cos\gamma$$

The internal stresses in the material are:

$$\sigma = \frac{KM_{res}x}{I}$$

$$\tau = \frac{KT_\theta x}{J}$$

The principle stresses $\sigma_{1,2}$ are:

$$\sigma_{1,2} = \frac{\sigma}{2} \pm \sqrt{\left(\frac{\sigma}{2}\right)^2 + \tau^2}$$

The von Mises stress σ_{vm} is:

$$\sigma_{vm} = \sqrt{(\sigma_1)^2 - \sigma_1\sigma_2 + (\sigma_2)^2}$$

A stand-alone MATLAB program has been developed to compute the stress condition with the above governing equations on each revolution of the coil along the lead midline curvature. By superimposing the normal and shear stress components resulting from bending and tensile elongation, the algorithm can be used to compute the stress condition for the implanted lead at all frames of motion (shown in result).

RESULTS

Implant Configurations

The open-coil lead of the first implanted micropacemaker dummy was inadvertently snagged on the end of the sheath during deployment, resulting in a permanent kink of the lead that made it impossible to quantify its configuration due to the limited fluoroscopy resolution. The body of the second pacemaker was released outside the pericardium, leaving the lead to bridge through the pericardial space to the myocardial electrode. This resulted in the pattern of stretch and offset of the lead that provided a useful

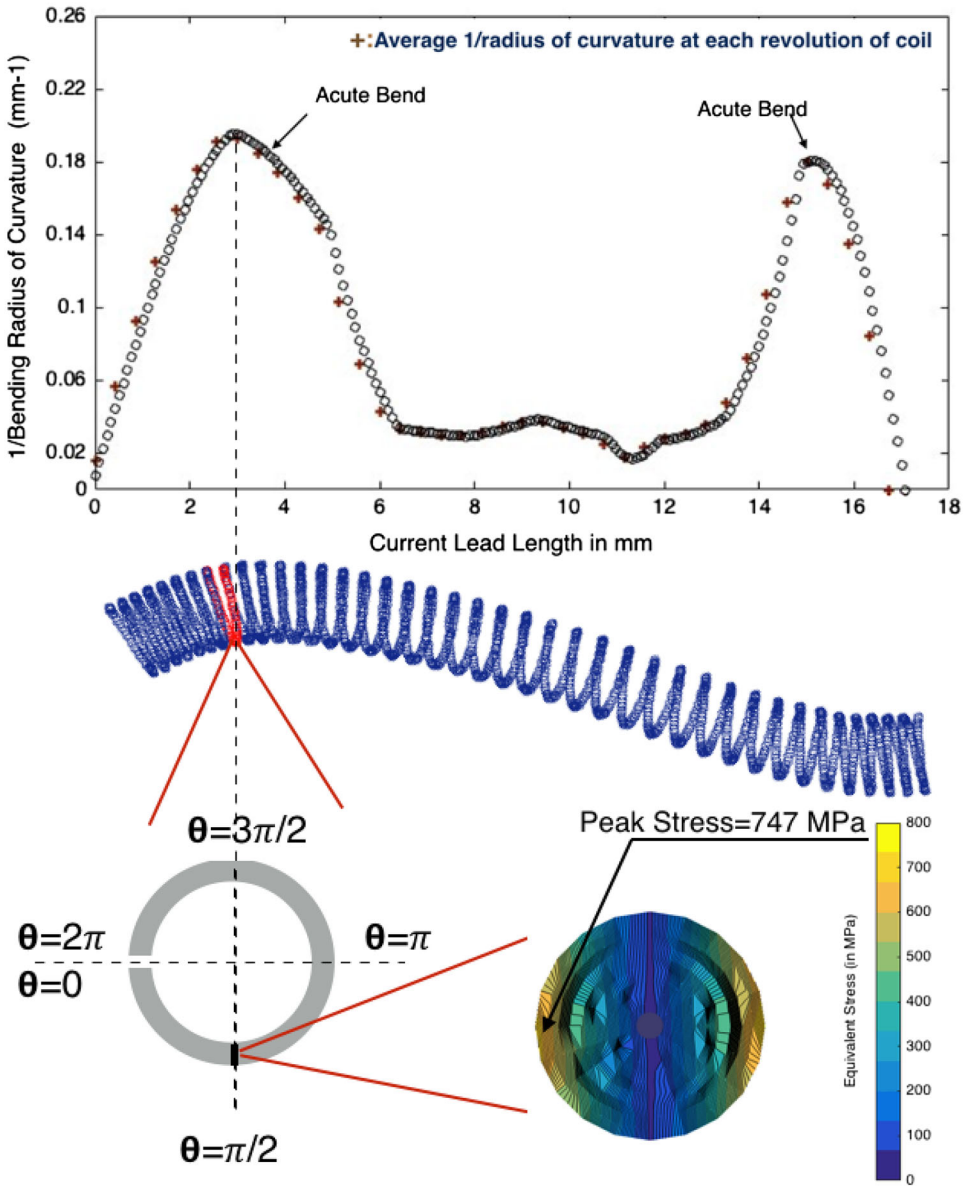

FIGURE 7. Analysis of the condition for which the maximal von Mises stress (747 MPa) was computed: Frame 7 (corresponding to maximal extension from Fig. 6), Turn 8 (point of maximally sharp bending radius located 3 mm from the Ir electrode end of the lead), $\theta = \pi/2$ rad (inside edge of bend in the coiled lead) and $\gamma = 0$ or π rad (compressed and extended sides of the solid SS wire). The open-coiled lead in blue: the lead was evenly stretched to 17 mm then deformed according to the bending radius of curvature on each turn of the coil.

case study for our analytical methods. The general configurations inferred from the radiographic images were confirmed at necropsy (Fig. 5). The wire coils of the lead were entirely embedded in a sleeve of mature fibrous, minimally-reactive connective tissue that was distinctive and easily separated from the surrounding membranes and structures. Adjacent coils were separated by a thin layer of connective tissue, preventing chafing of the thin Parylene insulation. The helical electrode was well-anchored in the myocardium by an inner core of connective tissue with its outer surface positioned close to healthy appearing myocytes.

Implanted Lead Geometric Deformation

The overall elongation of the implanted lead during one cardiac cycle is illustrated in Fig. 6. The result suggested that the implanted lead was constantly under tension with a peak length of 17 mm at Frame 7. The original resting length of the lead was 10 mm, so the

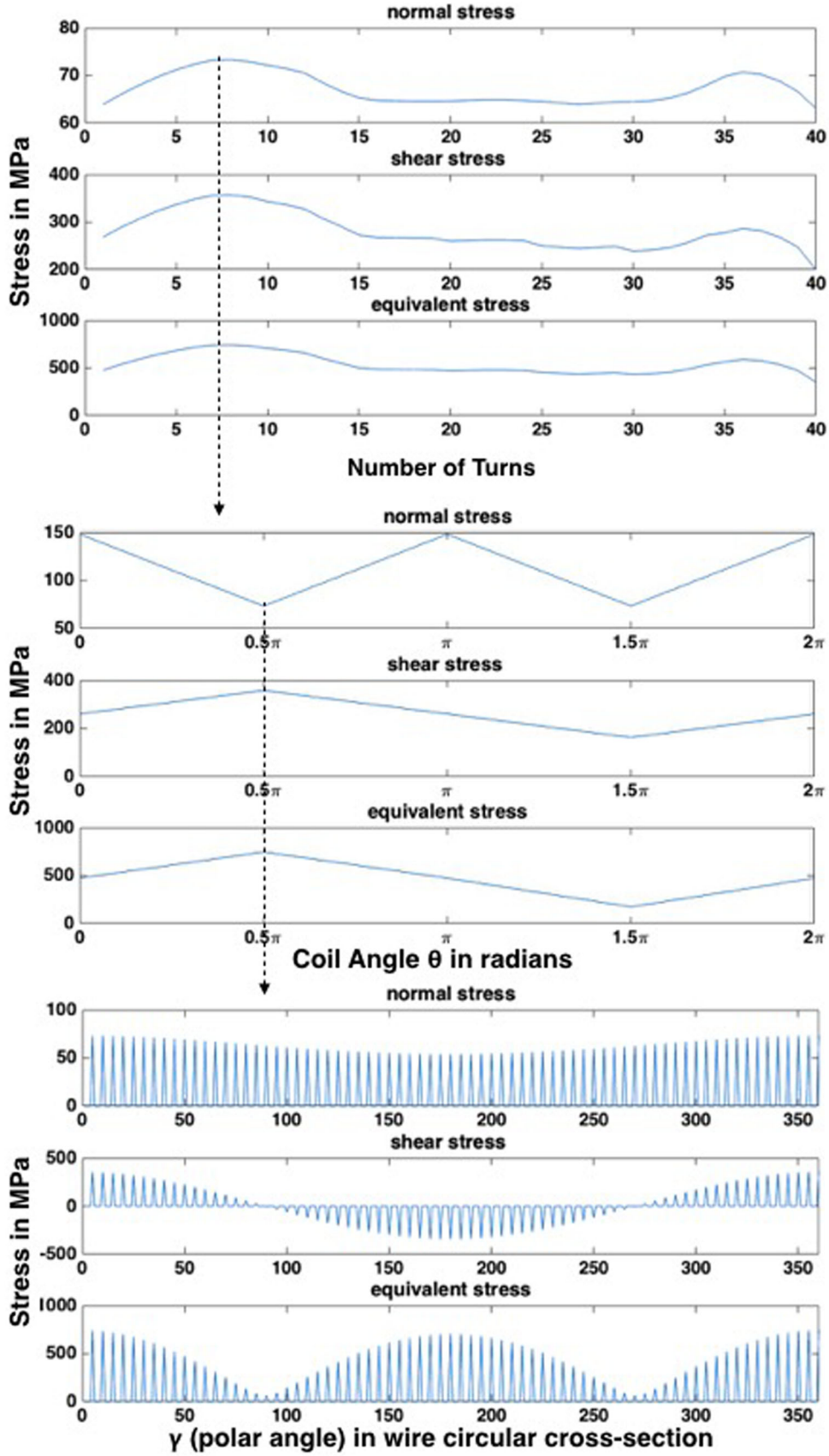

◀ **FIGURE 8. Top: The equivalent stress (von Mises stress), normal stress and shear stress distribution *vs.* the γ turns ($\theta = \pi$ /2, *di* = 76.2 μm (wire outer radius), $\gamma = 0$, frame #7). Middle: The equivalent stress (von Mises stress), normal stress and shear stress distribution *vs.* the θ (theta) rotation (turn = 8, *rx* = 76.2 μm (wire outer radius), $\gamma = 0$, frame #7). Bottom: The equivalent stress (von Mises stress), normal stress and shear stress distribution *vs.* the γ (gamma) rotation [turn = 8, $\theta = \pi$ /2, *rx* = 76.2 μm (wire outer radius), Frame #7].**

elongation at this frame was 7 mm. The inverse of the 3D radius of curvature at frame 7 is plotted in Fig. 7 as a function of the distance along the lead (as illustrated under the x-axis).

Stress Analysis

The maximum equivalent (von Mises) stresses and shear stresses occurred during maximal extension in Frame 7 (Fig. 6) and at Turn 8 along the lead where the radius of curvature of bending of the lead was sharpest (Fig. 7). A complete analysis of the contributions of normal and shear stress is presented as a function of θ (position around turn 8) and γ (polar angle at surface of circular wire cross-section) in Fig. 8. From radiographic and dissection images, the location with maximum equivalent stress is close to the position where the lead exits the pericardial tissue plane.

DISCUSSION

The analytical method presented here can be used to infer stress in a helical coil lead from readily available radiographic images of a beating heart. It assumes that strains are smoothly distributed among the turns of the coil, which are themselves not individually resolvable in the images. Given this limitation, the stress prediction may under-predict actual stress conditions in the individual coils if they are subject to local forces or deformations that would cause uneven distribution of strain among the turns. In addition, the method of 3D reconstruction of the implanted lead requires further verification to inform on the data error magnitude.

Inferring Lead Life from Stress Analysis

In the example analyzed here, the strains of the coil were potentially influenced by the transepicardial configuration of the lead, resulting in maximum stresses (Mean Stress = 531.4 MPa; Alternating Stress = ± 216.4 MPa). Most of the peak stress arose from the peak curvature in the sigmoidal configuration of the lead. This configuration can only arise if there are substantial translational forces on the anchor points at either end of the coil, *i.e.* the body of the pacemaker and the myocardial corkscrew electrode. We speculate that the lead would have assumed a much straighter configuration if the system were deployed entirely within the subpericardial space, but that remains to be tested in future experiments. The analytical method described herein is suited to estimating von Mises stresses that arise from any combination of tensile and bending strains on the helical lead. We assume that a smooth, cylindrical pacemaker body would not impose significant torsional strains on the helical lead.

Fatigue characterization of the 304SS wire coil has not yet been performed. It is noted that the fatigue strength of the wire itself is a function of the composition of the metal alloy, microstructure, surface condition, and processing to which the wire is subjected to form the coil lead.[16] The amount of drawing required to reach a particular wire diameter significantly increases the mechanical strength and fatigue strength of the material.[2] In order to complete a fatigue assessment for the pacemaker lead, tensile testing and fatigue characterization testing will be required for the actual wire used for the pacemaker lead. The wire coil fatigue data will be used in conjunction with the predicted stress conditions within the coil to determine if the pacemaker lead will survive the targeted 200 million cycles over a 5 year implant duration.

Adaptive Stabilization by Connective Tissue

In order to obtain long-term functionality of the epicardial micropacemaker system, the flexible lead must accommodate millions of flexion motions. As described above, our epicardial micropacemaker flexible lead is a short open-coil design that is intended to avoid stress-risers that occur when conventional polymeric encapsulants become embrittled and fracture.[3,6,12,13] The dimensions of the wire and coil that formed our prototype open-coil lead were chosen by intuition rather than engineering analysis of the composite material that arises when the spring-like coil is embedded in elastic connective tissue. Biological connective tissues tend to have nonlinear stress–strain relationships because of the complex shapes of the proteinaceous filaments from which they are composed.[15] Finite element analysis of the composite material will require a quantitative description of the connective tissue that actually forms around the coils. This could be obtained by comparing the strains produced in the coils when stressed statically in their bare vs. tissue-embedded form. We have successfully used microcomputed X-ray tomography to resolve the individual turns of the coiled leads under such static conditions *in vitro*. Such methods could be used to investigate systematically how the elastic properties of

the composite material change with factors such as dimensions of the wire coil, polymeric encapsulants with different adhesion to connective tissue, and elution of anti-inflammatory agents such as steroids, which are commonly added to cardiac electrodes to modify the foreign body reaction.[8]

ACKNOWLEDGEMENT

This research was funded by a NIH R01 Grant (1R01HD075135). Some aspects of the mechanical design and fabrication are the subjects of patents as well as pending patent applications assigned to Children's Hospital Los Angeles and University of Southern California. No commercial partnerships have yet been arranged.

CONFLICT OF INTEREST

Author Li Zhou, Yaniv Bar-Cohen, Raymond A. Peck, Giorgio V. Chirikian, Brett Harwin, Ramen H. Chmait, Jay D. Pruetz, Michael J. Silka, Gerald E. Loeb declare that they have no conflict of interest.

HUMAN AND ANIMAL ETHICS

No human studies were carried out by the authors for this article. All institutional and national guidelines for the care and use of laboratory animals were followed and approved by the appropriate institutional committees.

REFERENCES

[1]Altman, P. A., J. M. Meagher, D. W. Walsh, and D. A. Hoffmann. Rotary bending fatigue of coils and wires used in cardiac lead design. *J. Biomed. Mater. Res.* 43(1):21–37, 1998.

[2]Bhonsle, S., and C. Van Karsen. Mechanical and fatigue properties of stress relieved type 302 stainless steel wire. *J. Mater. Eng. Perform.* 1(3):363–369, 1992.

[3]de Voogt, W. G. Pacemaker leads: performance and progress. *Am. J. Cardiol.* 83(5):187–191, 1999.

[4]Durelli, A., V. Parks, and H. Hasseem. Helices under load. *J. Manuf. Sci. Eng.* 97(3):853–858, 1975.

[5]Fortescue, E. B., C. I. Berul, F. Cecchin, E. P. Walsh, J. K. Triedman, and M. E. Alexander. Patient, procedural, and hardware factors associated with pacemaker lead failures in pediatrics and congenital heart disease. *Heart Rhythm.* 1(2):150–159, 2004.

[6]Furman, S., D. L. Hayes, and D. R. Holmes. A Practice of Cardiac Pacing. Oxford: Wiley-Blackwell, 1989.

[7]Juvinall, R. C., and K. M. Marshek. Fundamentals of Machine Component Design. New York: Wiley, 2006.

[8]Kistler, P. M., G. Liew, and H. G. Mond. Long-term performance of active-fixation pacing leads: a prospective study. *Pacing Clin. Electrophysiol.* 29(3):226–230, 2006.

[9]Loeb, G. E., L. Zhou, K. Zheng, A. Nicholson, R. A. Peck, A. Krishnan, *et al.* Design and testing of a percutaneously implantable fetal pacemaker. *Ann. Biomed. Eng.* 41(1):17–27, 2013.

[10]Malvern, L. E. Introduction to the Mechanics of a Continuous Medium. Englewood Cliffs: Prentice-Hall, 1969.

[11]Meagher, J. M., and P. Altman. Stresses from flexure in composite helical implantable leads. *Med. Eng. Phys.* 19(7):668–673, 1997.

[12]Phillips, R., M. Frey, and R. O. Martin. Long-term performance of polyurethane pacing leads: mechanisms of design-related failures. *Pacing Clin. Electrophysiol.* 9(6):1166–1172, 1986.

[13]Podnos, E., E. Becker, J. Klawitter, and P. Strzepa. FEA analysis of silicone MCP implant. *J. Biomech.* 39(7):1217–1226, 2006.

[14]Silka, M. J., and Y. Bar-Cohen. Pacemakers and implantable cardioverter-defibrillators in pediatric patients. *Heart Rhythm.* 3(11):1360–1366, 2006.

[15]Silver, F., Y. Kato, M. Ohno, and A. Wasserman. Analysis of mammalian connective tissue: relationship between hierarchical structures and mechanical properties. *J Long Term Effects Med. Implants* 2(2–3):165–198, 1991.

[16]Wahl, A. M. Mechanical Springs. Cleveland: Penton Publishing Company, 1944.